Improving Modal Parameter Predictions for Jointed Airframe Panels. Part II: Improved Numerical Model

Seong-Ho Yun
Post-doctoral Associate
Department of Mechanical Engineering
Aeronautical Engineering and Mechanics.
Rensselaer Polytechnic Institute
Troy, New York

Olivier A. Bauchau
Professor
School of Aerospace Engineering
Georgia Institute of Technology
Atlanta, Georgia

A companion paper has described an experimental investigation aimed at identifying the physical mechanisms and modeling errors that are the culprits for the lack of correlation between experimental measurements and analytical predictions of the modal parameters of helicopter airframes. Large discrepancies were observed between measured and predicted natural frequencies that can be primarily assigned to the modeling errors associated with current industry practices. The present paper focuses on the development of simple, improved numerical models based on a lumped parameter approach which accounts for joint flexibilities by a set of concentrated linear and torsional springs whose stiffnesses are determined experimentally. In the proposed finite element model, the joint compliance is represented by beams of a circular cross-section whose diameter is evaluated from the measured joint stiffnesses. The frequencies predicted by this proposed numerical model were compared with the measured frequencies for panels with various types of joints and improved correlation was found when compared with current industry modeling practices.

Introduction

A companion paper (Ref. 1) has described an experimental investigation aimed at identifying the physical mechanisms and modeling errors that are the culprits for the lack of correlation between experimental measurements and analytical predictions of the modal parameters of helicopter airframes. The identification of the major contributors to this lack of correlation is an indispensable first step in improving numerical models. The study focused on simple configurations: panels with lap and butt joints fastened with HI-LITE fasteners or rivets. Natural frequencies predicted using the reinforcing beam or double thickness methods, two current industry modeling practices, were found to overestimate the natural frequencies measured using impact hammer tests by up to 40%. On the other hand, measured and predicted mode shapes were found to correlate closely.

In view of this experimental evidence, the lack of correlation between experimental results and numerical predictions for natural frequencies can be almost entirely assigned to errors associated with current industry modeling practices. Indeed both reinforcing beam and double thickness methods grossly overestimate the joint stiffness. On the other hand, other mechanisms, such as damping and nonlinearities, will further affect forced response. In this paper, the focus is on improving natural frequency predictions, and as a result, improving modeling practices will be the primary concern.

One way of improving the reliability of the models would be to perform very detailed, three dimensional analyses of the joint area. Such endeavor would be very costly from a computational standpoint, and it is not clear that the accurate deformation modes and the relevant contributing physical mechanisms that determine the overall joint stiffness can be identified based on numerical studies only. Even if successful, this approach might not be practical when dealing with actual airframes: a detailed model of all the joints in the entire helicopter structure would clearly be beyond the reach of even the most powerful computers.

An alternate, *lumped parameter* approach, will be investigated in this paper. More specifically, joint flexibilities will be represented in the numerical model by a set of concentrated linear and torsional springs whose stiffnesses are determined experimentally. The approach proceeds in two steps: first, the global stiffness characteristics of joints are evaluated experimentally using simple test articles; then, these measured stiffnesses are incorporated in a simple numerical model to represent the overall effect of the joint. The first step of the procedure involves the design a simple experiment to evaluate joint stiffnesses. This simple experiment will be described in section 3. Section 4 will introduce the simple, improved numerical model that uses these experimentally measured stiffnesses as a means of representing effective joint compliance to improve the correlation between predicted and measured natural frequencies.

Analytical Background

The conceptual basis for the determination of the stiffness of a joint is to consider a clamped-clamped beam of length $2L$. The beam is cut at mid span, then two springs are added at this cut: a linear spring of stiffness k and a torsional spring of stiffness g. These two springs form the lumped parameter representation of a joint placed at the beam's midspan. The beam without joint corresponds to infinite spring constants, i.e. $k \rightarrow \infty$ and $g \rightarrow \infty$.

Manuscript received Jan. 1997; accepted Jan, 1998.

Eigenanalysis of a cantilever beam with tip springs

The symmetric modes of the clamped-clamped beam with midspan springs are identical to those of a cantilevered beam of length L with a tip torsional spring of constant g. On the other hand, the anti-symmetric modes are identical to those of a cantilevered beam of length L with a tip linear spring of constant k.

The boundary conditions for a cantilevered beam of length L with a tip torsional spring of constant g are

$$\begin{aligned} &@\eta = 0:\ \Phi(0) = 0,\ \Phi'(0) = 0; \\ &@\eta = 1:\ \Phi''(1) + \mathcal{G}\Phi'(1) = 0;\ \Phi'''(1) = 0, \end{aligned} \tag{1}$$

where $\eta = x/L$ is the nondimensional spanwise variable along the axis of the beam, $\Phi(\eta)$ the transverse deflection, and $(.)'$ denotes a derivative with respect to η. The nondimensional tip torsional spring stiffness $\mathcal{G}$ is defined as

$$\mathcal{G} = \frac{gL}{EI}, \tag{2}$$

where EI is the bending stiffness of the beam.

For the cantilevered beam of length L with a tip linear spring of constant k, the corresponding boundary conditions are

$$\begin{aligned} &@\eta = 0:\ \Phi(0) = 0,\ \Phi'(0) = 0; \\ &@\eta = 1:\ \Phi'''(1) - K\Phi(1) = 0;\ \Phi''(1) = 0, \end{aligned} \tag{3}$$

where the nondimensional tip linear spring stiffness K is defined as

$$K = \frac{kL^3}{EI}. \tag{4}$$

Under the assumptions of classical Euler-Bernoulli beam theory, small amplitude transverse vibrations are described by the following equation

$$\Phi_i(\eta) = c_1 \sin\beta_i\eta + c_2 \cos\beta_i\eta + c_3 \sinh\beta_i\eta + c_4 \cosh\beta_i\eta \tag{5}$$

where the four integration constants c_1, c_2, c_3 and c_4 are to be determined by four boundary conditions, and β_i is the nondimensional frequency parameter, related to the dimensional circular frequency ω_i as

$$\omega_i = \beta_i^2 \sqrt{\frac{EI}{mL^4}} \tag{6}$$

The frequency equation is then obtained by evaluating the integration constants with the help of the boundary conditions and requiring the existence of a nontrivial solution. This leads to

$$[1 + \cos\beta_i \cosh\beta_i] + \mathcal{G}\,[\sin\beta_i \cosh\beta_i + \cos\beta_i \sinh\beta_i] / \beta_i = 0; \tag{7}$$

and

$$[1 + \cos\beta_i \cosh\beta_i] + K\,[\sin\beta_i \cosh\beta_i - \cos\beta_i \sinh\beta_i] / \beta_i^3 = 0; \tag{8}$$

for the cantilevered beam with tip torsional and linear springs, respectively. The first bracketed terms of these equations represent the frequency equation for a cantilever beam that is free at the tip, whereas the second bracketed terms represent the frequency equations for cantilevered beam with tip rotational or translational restraints, respectively.

Eqs. (7) and (8) give the spectrum of frequencies as a function of the stiffness of the torsional and linear springs, respectively. Natural frequencies were found to be very sensitive to the spring stiffness magnitude in the range of stiffnesses between 10^{-1} and 10^3. For nondimensional stiffnesses below 10^{-1} frequencies remained practically constant and equal to the frequencies of a cantilevered beam without tip springs. On the other hand, for nondimensional stiffnesses above 10^3, the frequencies were constant once more, and equal to those of a cantilevered beam with tip torsional or linear restraints. Mode shape tip amplitude and slope were also found to be very sensitive to the spring stiffness magnitude in the same range. It was noted that the tip slope sensitivities are larger than either tip deflection or frequency sensitivities.

In Ref. 1, the experimentally measured frequencies of fastened and riveted plates were found to differ significantly, showing the dependency of natural frequencies on joint stiffness characteristics. This indicates that typical joint stiffnesses fall within the range of 10^{-1} to 10^3.

Numerical sensitivities

The simplified analytical model described in the previous section does not take into account the added mass associated with the overlapping material in the joint area. This added mass is of course critical for an accurate prediction of the natural frequencies for the symmetric modes which maximum deflection are at midspan. A simple ABAQUS model was used to obtain numerical predictions of modal parameter sensitivities. The finite element model of the double cantilevered beams consists of 25 cubic beam elements, and that of the joint consists of linear and torsional spring elements placed at the beam's midspan, and lumped masses to account for the added mass. The beam elements do not account for shearing deformations.

Predictions were made for cantilevered and double cantilevered beams, denoted *CF* and *CC*, respectively. Double cantilevered beams with midspan lap joints fastened with HI-LITEs or rivets are denoted *LH* and *LR*, respectively, and double cantilevered beams with midspan butt joints fastened with HI-LITEs or rivets, denoted *BH* and *BR*, respectively. Frequencies computed for the lowest six modes are summarized in Table 1 for infinite values of the linear and torsional midspan springs. With this crude representation of the structure, the numerical model does not distinguish between the two types of fastener and identical frequencies are obtained for both cases. As expected, the frequencies for the symmetric modes (*i.e.* modes 1, 3, and 5) of the jointed beam are lower than those of the *CC* configuration because of the added mass. For the anti-symmetric modes (*i.e.* modes 2, 4, and 6), the midspan mass only contributes rotary inertia, a negligible effect. The sensitivities predicted by this numerical model are presented in Figs. 2 to 9, and will be discussed in the next section, together with the corresponding experimentally measured sensitivities.

Table 1. Numerical predictions of the reference natural frequencies for jointed beams [Hz].

	1ST MODE	2ND MODE	3RD MODE	4TH MODE	5TH MODE	6TH MODE
CF	45.51	285.26	799.15			
CC	72.41	199.60	391.33	647.09	967.09	1351.90
LH and *LR*	69.07	199.53	378.05	646.91	935.54	1349.00
BH and *BR*	64.80	201.32	355.19	648.98	881.45	1341.60

Experimental Determination of Joint Stiffnesses

In the previous section, the modal characteristics of double cantilevered beam were shown to be quite sensitive to the stiffness of midspan torsional and linear springs. This observation provides the means of experimentally measuring these stiffnesses: first, the sensitivities of modal characteristics are determined experimentally, then analytical tools are used to compute the corresponding midspan stiffnesses.

Experimental set-up

The cantilevered (*CF*) and double cantilevered (*CC*) beams have a width of 0.9 *in* and length of 8 and 16 *in*, respectively. The jointed samples had a length of 16 *in* and a width of 0.9 *in*, and were tested in the fixture depicted in Fig. 2 of Ref. 1. The testing equipment is described in section (2.3) of Ref. 1. All test articles were made of thin 5052 aluminum sheets and the following nominal values of the physical properties were used: Young's modulus $E = 1.015 \times 10^7$ *psi*, Poisson's ratio $\nu = 0.33$, and density $\rho = 0.097$ *lbs/in*^{3}. The sheets had a nominal thickness $t = 0.09$ *in*.

Shaker tests were conducted to determine the modal characteristics of all samples. Natural frequencies, and mode shape midspan deflections and slopes were measured for the lowest five modes of the structures. The shaker was attached to the sample at 0.75 *in* from the left clamped support.

In order to measure consistent mode shape deflections and slopes, the excitation force level must be properly chosen to assure that the structure is excited in its linear range. Figure 1 presents transfer accelerances versus excitation force level for various types of samples. The transfer accelerance is evaluated from the excitation forces and midspan acceleration. For the *CC* sample, the measured accelerance is about constant over the entire range of excitation force. In contrast, for the samples with midspan joints the accelerance response shows three distinct regions which can be explained by the following arguments. At low levels of excitation (region I), the force level is so low that friction forces in the joint are sufficient to prevent any relative motion of the joint's components. As the excitation is increased (region II), the friction forces are no longer large enough to prevent all relative motions causing increases in accelerance with increased excitation force level. Finally in region III, the excitation force is large enough to overcome all friction forces in the joint, and constant accelerance level is observed once again. This phenomenon is called ankylosis (Ref. 2). All tests were run with excitation forces of about 1.5×10^{-3} *lbf*, in the range where accelerance is independent of the excitation force level.

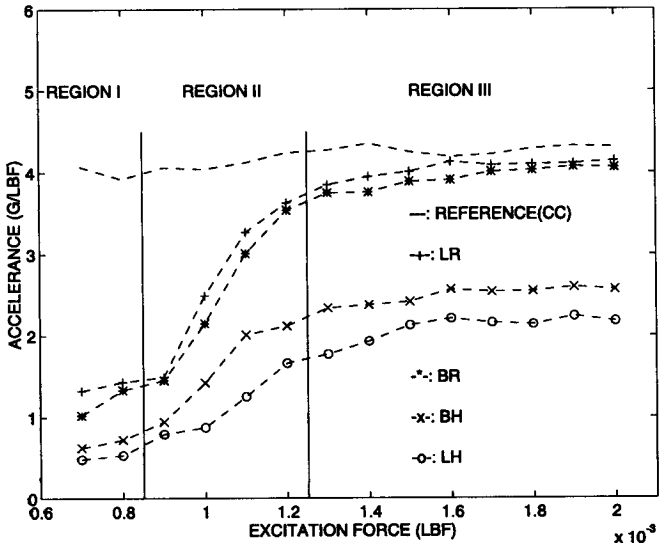

Fig. 1. Accelerance versus excitation force for various types of samples.

Stiffness Measurements Based on Natural Frequency Sensitivities

A first estimate of joint stiffness will be based on measurements of natural frequency sensitivities. For lap joints fastened with HI-LITEs and rivets natural frequencies were measured for the lowest three symmetric modes. Table 2 lists the frequencies measured in three independent tests, average frequencies, and the sensitivities based on the reference frequencies listed in Table 1 for the corresponding cases.

Figure 2 shows the frequency sensitivities predicted using the numerical model of section 2.2 as a function of the nondimensional torsional stiffness $\mathcal{G}$ for beams with lap joints. In all sensitivity plots presented here, sensitivities were set to zero for infinite values of joint stiffnesses. Joint stiffnesses can now be evaluated by entering the measured frequency sensitivities of Table 2 on the ordinate and reading the corresponding nondimensional stiffness on the abscissa. After averaging, the measured joint stiffnesses are $\mathcal{G} = 3.79$ and $\mathcal{G} = 13.4$ for the joints fastened with HI-LITEs and rivets, respectively. The corresponding dimensional stiffnesses are then obtained from eq. (2) as $g = 263$ *in lbf* and $g = 927$ *in lbf*, respectively. Note that in view of the logarithmic scale used for the abscissa, the measured joint stiffnesses are quite inaccurate for small frequency sensitivity values.

Table 2. Natural frequency sensitivities for lap joint beams fastened with HI-LITEs and rivets.

	LH			*LR*		
	1ST MODE	3RD MODE	5TH MODE	1ST MODE	3RD MODE	5TH MODE
TEST I	60.50	340.00	820.10	67.21	357.40	847.70
TEST II	59.90	329.70	818.40	68.00	361.30	849.20
TEST III	61.40	342.10	823.40	69.39	363.40	860.30
AVERAGE	60.60	337.27	820.60	68.20	360.70	852.40
SENSITIVITY	–12.3%	–10.8%	–12.3%	–1.25%	–4.59%	–9.78%

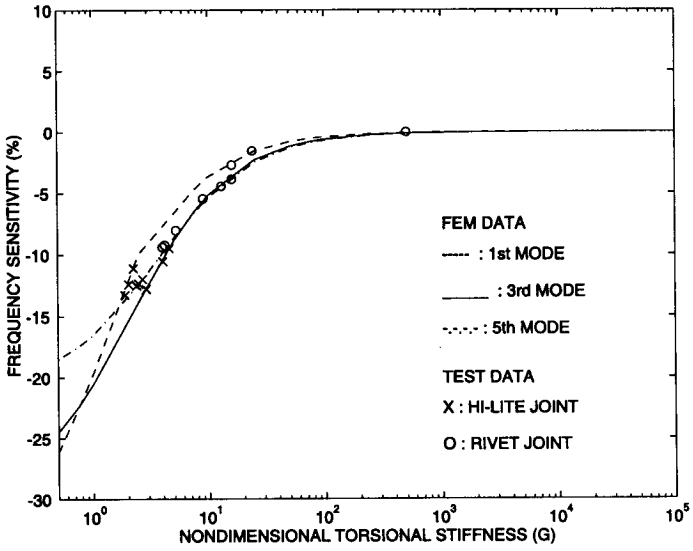

Fig. 2. Predicted natural frequency sensitivities as a function of nondimensional joint torsional stiffness for lap joints.

Similar measurements were made for the anti-symmetric modes of the beam, and the linear stiffness of the joints can be estimated from these measurements. Figure 3 shows the numerically predicted frequency sensitivities as a function of the nondimensional linear stiffness K for beams with lap joints. With the help of the procedure described above, the linear stiffnesses of the joint are estimated as $K = 767$ and $K = 1070$ for the joints fastened with HI-LITEs and rivets, respectively. As expected, the estimated linear and torsional stiffnesses are higher for riveted joints than for joints fastened with HI-LITEs.

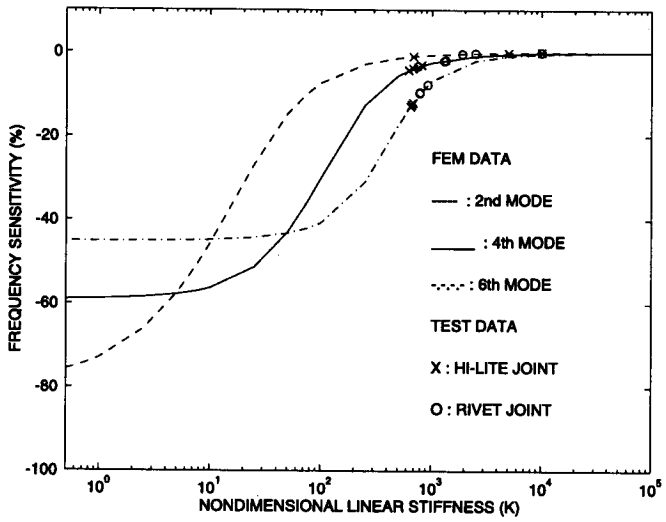

Fig. 3. Predicted natural frequency sensitivities as a function of nondimensional joint linear stiffness for lap joints.

The torsional and linear stiffnesses of butt joints can be estimated in a similar manner. Figures 4 and 5 show the numerical sensitivity predictions and test results for the torsional and linear stiffnesses, respectively.

Stiffness measurements based on mode shape tip deflection and slope sensitivities

The results of the previous section clearly show that small experimental errors in measured frequency sensitivities lead to large errors in estimations of joint stiffnesses. More accurate estimates can be obtained by taking into consideration mode shape deflection and slope sensitivities.

Mode shape deflections were measured at a point located 7 *in* from the left clamp of the beam, *i.e.* 1 *in* to the left of the midspan location. Representative results are shown Figs. 6 and 7 for the estimation of the linear stiffness of lap joint and torsional stiffness of butt joints, respectively. Both deflections and slopes were normalized as percent changes in the deflections and slopes of the continuous beam due to addition of a joint.

Mode shape slopes were measured as differential mode shape deflections. For symmetric modes, amplitudes were measured at points located

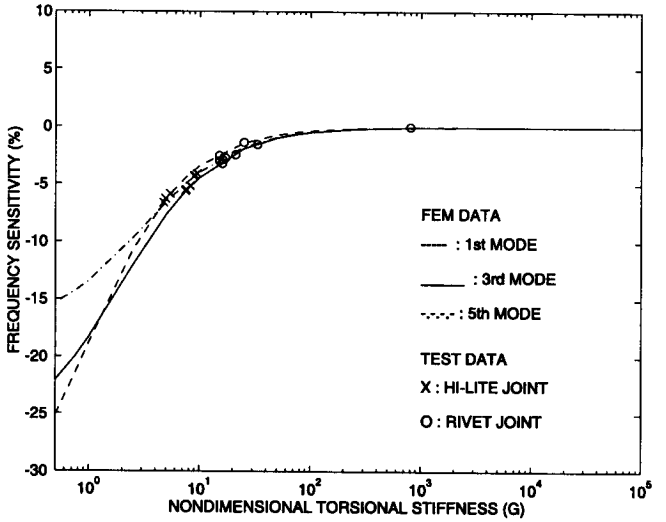

Fig. 4. Predicted natural frequency sensitivities as a function of nondimensional joint torsional stiffness for butt joints.

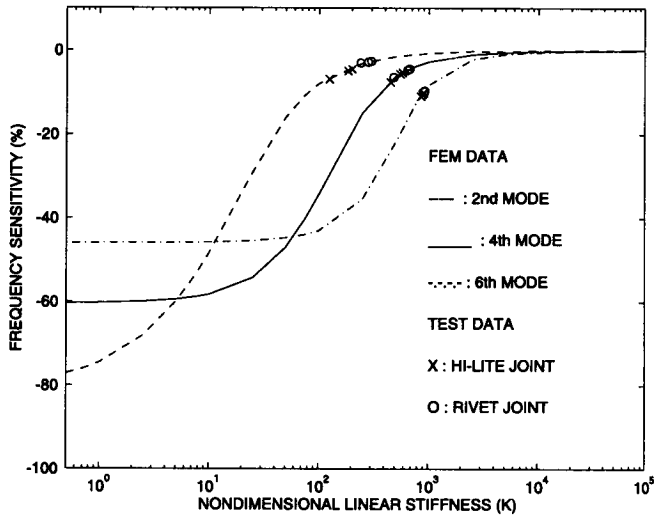

Fig. 5. Predicted natural frequency sensitivities as a function of nondimensional joint linear stiffness for butt joints.

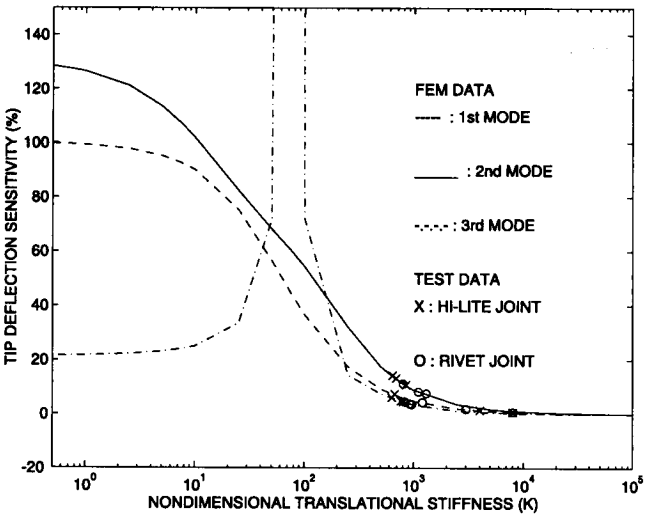

Fig. 6. Predicted mode shape deflection sensitivities as a function of nondimensional joint linear stiffness for lap joints.

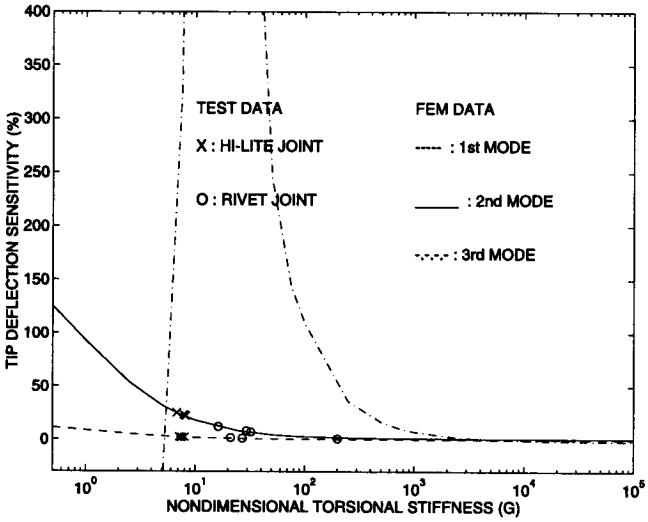

Fig. 7. Predicted mode shape deflection sensitivities as a function of nondimensional joint torsional stiffness for butt joints.

7 and 8 *in* from the left clamp of the beam yielding an estimate of the slope on the left of the midspan point. For anti-symmetric modes, amplitudes were measured at points located 7.5 and 8.5 *in* from the left clamp of the beam yielding an estimate of the mid-span slope. Representative results are shown Figs. 8 and 9 for the estimation of the torsional stiffness of lap joint and linear stiffness of butt joints, respectively.

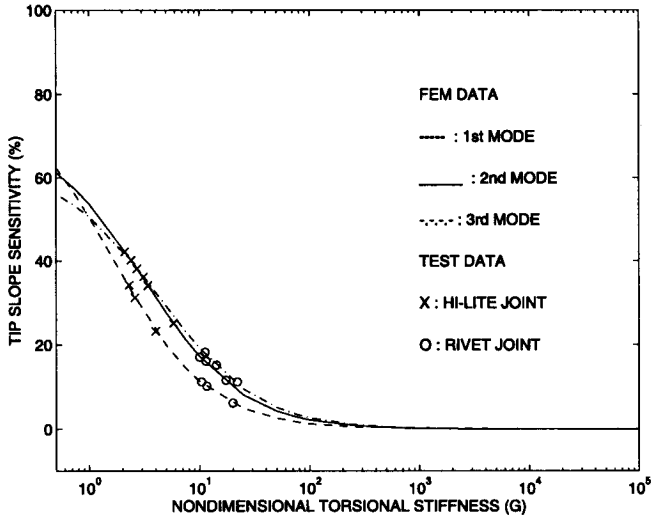

Fig. 8. Predicted mode shape slope sensitivities as a function of nondimensional joint torsional stiffness for lap joints.

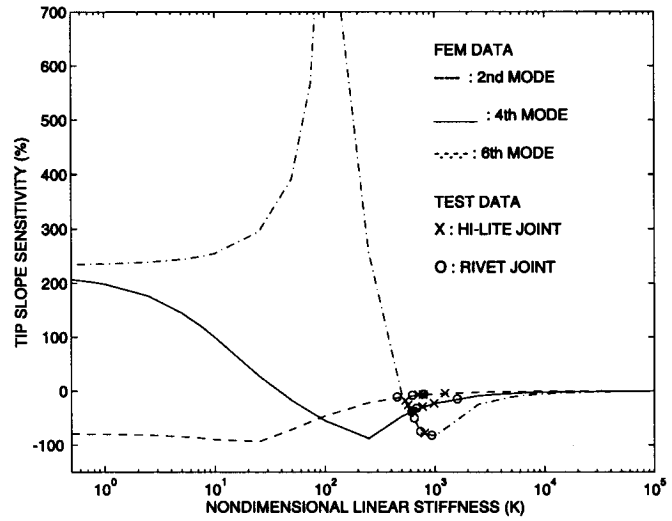

Fig. 9. Predicted mode shape slope sensitivities as a function of nondimensional joint linear stiffness for butt joints.

Summary of joint stiffness measurements

The results obtained from sensitivity measurements for frequencies, mode shape tip deflections, and mode shape tip slopes are summarized in Table 3 for the various types of test samples. Estimates of the joint stiffnesses calculated from the various measurements were found to be in reasonable agreement. The nondimensional torsional spring stiffness of the samples fastened with HI-LITEs were found to be significantly lower than for those samples fastened with rivets. A similar decrease is observed in the linear spring stiffness, though it is not as pronounced. Average joint stiffnesses based on the three types of measurements are listed in the last column of Table 3.

Table 3. Summary of joint stiffness estimates based on sensitivity measurements for frequencies, mode shape deflections, and mode shape slopes.

	Estimates based on measurements of			
	Frequency	Tip deflection	Tip slope	AVERAGE
LH (G)	3.79	3.47	4.33	3.86 (g = 268 *in lbf*)
LH (K)	767	720	788	758 (k = 822 *lbf/in*)
LR (G)	13.4	12.8	12.2	12.8 (g = 887 *in lbf*)
LR (K)	1070	1010	940	1010 (k = 1095 *lbf/in*)
BH (G)	7.65	7.16	7.81	7.54 (g = 523 *in lbf*)
BH (K)	620	6.93	971	761 (k = 825 *lbf/in*)
BR (G)	48.0	15.0	13.3	25.4 (g = 1760 *in lbf*)
BR (K)	670	976	996	880 (k = 955 *lbf/in*)

Improved Numerical Model

The joint stiffnesses evaluated in the previous section for simple beam samples were used to develop an improved finite element model for jointed panels. The predictions of this improved model will then be compared with the measured frequencies for panels with various types of joints, as reported in Ref. 1.

The finite element model

A schematic diagram of the finite element model of jointed panels is shown in Fig. 10. The panels are represented by plate elements located at the panel mid-plane, as are the splice plates. A fastener is represented by a number of short beam elements that connect the panels to the splice plates around the perimeter of the actual fastener hole. The use of beam elements to represent the joint stiffnesses is preferable to the use of concentrated springs as beams provide a means of representing the gap between the mid-planes of the panel and splice plates. Although small, this gap is important as it creates significant bending moments in the joint area. Three configurations will be investigated in this work depending on the number n of short beams used in the fastener model. The simplest model, $n = 1$, involves a single beam located at the center of the fastener. The other two models, $n = 4$ or $n = 8$, have four or eight beams equally spaced around the perimeter of the fastener hole, respectively.

The finite element model was implemented using the ABAQUS pack-

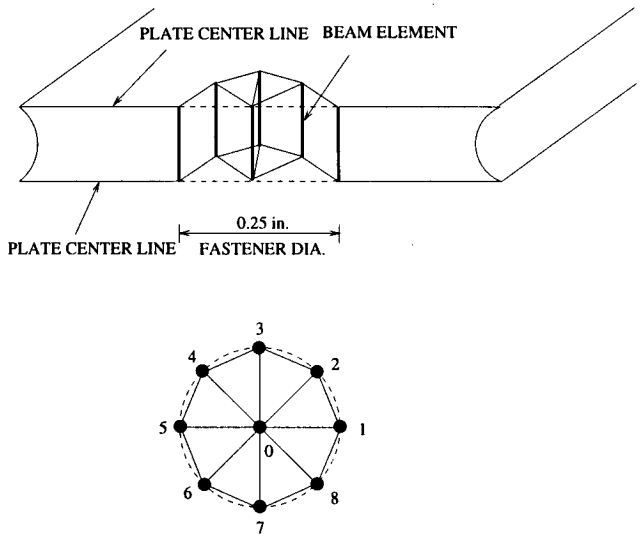

Fig. 10. Schematic of the finite element model in the joint area.

age. The panels and splice plates were modeled with four noded, shear deformable plate elements. The mesh corresponds to an assembly of square elements 1 *in* by 1 *in* in size. Both *h* and *p* refinement (Ref. 3) techniques were used to show that this mesh yielded converged results for the five lowest modes of the jointed panels, with discretization errors of less than 1%. The short beams were represented by shear deformable beam elements with a circular section of diameter d_e. The mass properties of the beam element were calculated to match the total fastener mass. The complete model presents two parameters, *n*, the number of connecting short beams, and d_e, the diameter of their circular cross-section.

Finite element model parameter adjustment

In section 3, equivalent linear and torsional joint stiffnesses have been evaluated experimentally based on simple beam-like configurations. These measured stiffnesses should be used to determine the values of the parameters of the finite element model, *n* and d_e, for more complex configurations, such as the jointed panels considered in Ref. 1. Unfortunately, this determination is not a straightforward process because the jointed panels are subjected to a combination of shear forces, axial forces and bending moments applied to the joint area. Furthermore, the relative magnitude of these various forces might differ from mode to mode.

Both lap and butt joints are subjected to a bending moment M acting in an unknown direction, a shear force F_s acting in a direction normal to the plane of the panel, and an axial force F_a acting in the plane of the panel. It should be noted that for lap joints, the shear force acts in a direction parallel to the fastener axis, whereas the axial force direction is transverse to the fastener axis. For butt joints, the situation is reversed. As a result, it is difficult to predict a unique value of stiffness in a specified direction, independent of other types of forces (Refs. 4, 5). Furthermore, the magnitude and extent of the prying action associated with the clamping force in the fastener are also difficult to evaluate (Ref. 6). Hence, the torsional and linear stiffnesses evaluated in section 3 should not be viewed as actual stiffness values but rather, the stiffness predictions based on the various measurement methods should be viewed as providing a range of reasonable values of joint stiffnesses.

Realistic estimates of the finite element model parameters *n* and d_e can be made with the help of simple, strength of material type arguments. First, consider the response of the joint area when subjected to sole bending moments. For *n* equally spaced cylindrical beams, the joint torsional stiffness *g* is

$$g = n\,\frac{E_e I_e}{L_e}, \tag{9}$$

where $Ie = \pi d_e^4/64$ is the second area moment of the beam's cross-section, L_e its length, E_e Young's modulus of the fastener material, and $E_e I_e/L_e$ the equivalent torsional stiffness of a single beam.Next, consider the response of the lap joint subjected to sole shearing forces. The joint linear stiffness *k* is

$$k = n\,\frac{E_e A_e}{L_e}, \tag{10}$$

where $A_e = \pi d_e/4$ the element cross-sectional area. Finally, for a butt joint subjected to sole shearing forces, the linear stiffness *k* is

$$k = n\,\frac{3E_e I_e}{L_e}, \tag{11}$$

In summary, the beam element diameter for lap joints can be evaluated in two different manners based on eqs. (9) or (10), to yield

$$d_e = 3.3582\sqrt[4]{\frac{G}{nE_e}};\ \text{or}\ \ d_e = 0.3524\sqrt[4]{\frac{K}{nE_e}}, \tag{12}$$

respectively, where the length of the beam element is L_e= 0.09 *in*, and the definition of the nondimensional joint stiffnesses Refs. 2 and 4 were used. Similarly, the beam element diameter for butt joints is found from eqs. (9) and (11) as

$$d_e = 3.3582\sqrt[4]{\frac{G}{nE_e}};\ \text{or}\ \ d_e = 0.2706\sqrt[4]{\frac{K}{nE_e}}, \tag{13}$$

respectively.

The estimated joint linear and torsional stiffnesses listed in Table 3 are now used to calculate the beam element diameters corresponding to the various joint configurations using Eqs. (12) and (13) for lap and butt joints, respectively. The results are listed in Table 4 for different values of *n*. Fastener Young's modulus was 16.0×10^6 and 10.4×10^6 *psi* for the HI-LITEs and rivets, respectively.

Table 4. Beam element diameter d_e estimated from the measured joint stiffnesses.

	d_e [$\times 10^{-3}$ *in*] estimates		
	n	based on G	based on K
LH	1	74	2.5
	4	53	1.2
	8	44	0.86
LR	1	110	3.5
	4	79	1.7
	8	67	1.2
BH	1	88	22
	4	62	16
	8	52	13
BR	1	130	26
	4	94	18
	8	79	15

Clearly, the measurements of joint stiffnesses only yield a range of likely values for the beam element diameters. These values can be fine-tuned based on the experimentally measured frequencies for jointed panels reported in Ref. 1. Figure 11 shows the normalized frequencies for the *L6D10H* lap joint panel as a function of d_e, for $n = 4$. The normalized frequencies shown on the ordinate are the frequencies computed by the finite element model divided by the experimentally measured frequency. The range of d_e shown in the figure is from 0.01 to 0.2 *in* whereas the likely range from Table 4 is from 0.0012 to 0.053 *in*. Frequencies computed with d_e values outside of the likely range are almost independent of d_e, as expected. Within the likely range, predicted frequencies are in best agreement for $d_e \approx 0.01$ *in*.

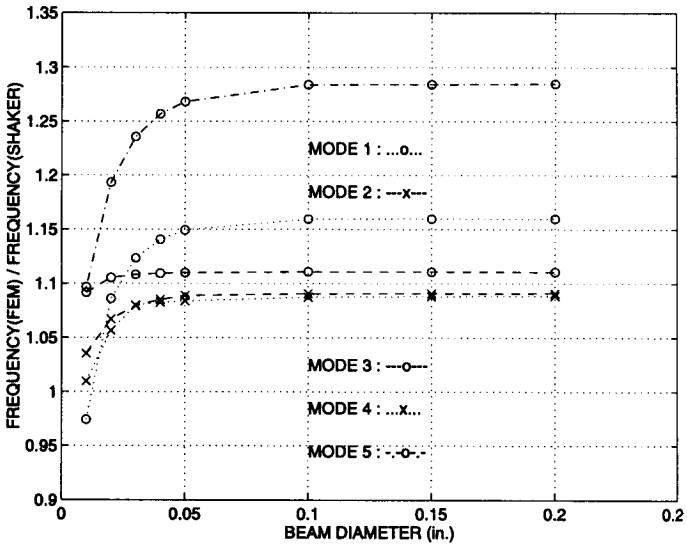

Fig. 11. Normalized frequencies versus d_e for the *L6D10H* panel ($n = 4$).

Similar studies can be performed for other types of joint configurations. Representative results are shown in Figs. 12, 13, and 14 for the *L6D10R*, *B4D2H*, and *B4D5R* configurations, respectively. It should be noted that over the likely range of beam diameter, the lowest three predicted frequencies are in fairly good agreement with the measurements and show little dependency on beam diameter. In other words, the beam diameter predicted by any joint stiffness measurement would yield good correlation with the lowest measured frequencies. Fine tuning only improves the correlation for the last two modes.

Table 5 lists the values of n and d_e yielding the best correlation with experimentally measured frequencies for the various panel configurations. It should be noted that for the lap joints, the optimal d_e value is close to that obtained based on the measured joint torsional stiffness G, whereas for butt joints the optimal d_e value is close to that obtained based on the measured joint linear stiffness K.

Correlation of the measured frequencies with the predictions of the improved finite element model

The frequencies predicted by the proposed finite element model described in the previous section will be compared with the measured frequencies reported in Ref. 1. The parameters of the finite element model are those listed in Table 5. Figure 15 shows the correlation between measured frequencies and those predicted by the DB-TH method (see Ref. 1) and by the proposed model for *L6D4H* and *L6D10H* panels. Errors of up to 40% are observed for the DB-TH methods, but are reduced to 5% for the proposed model.

Similar conclusions are drawn from Fig. 16 which shows the corre-

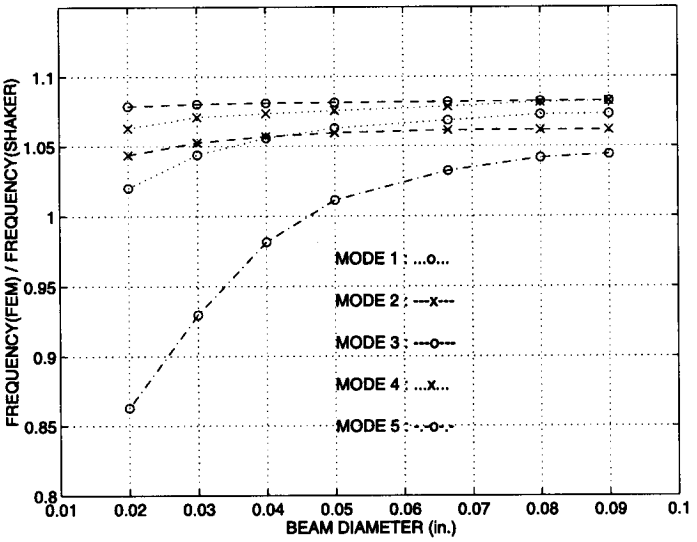

Fig. 12. Normalized frequencies versus d_e for the *L6D10R* panel (n = 8).

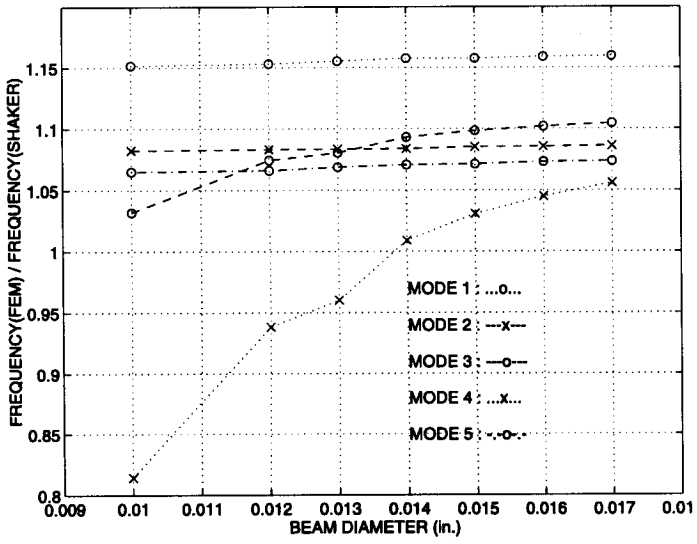

Fig. 13. Normalized frequencies versus d_e for the *B4D2H* panel (n =4).

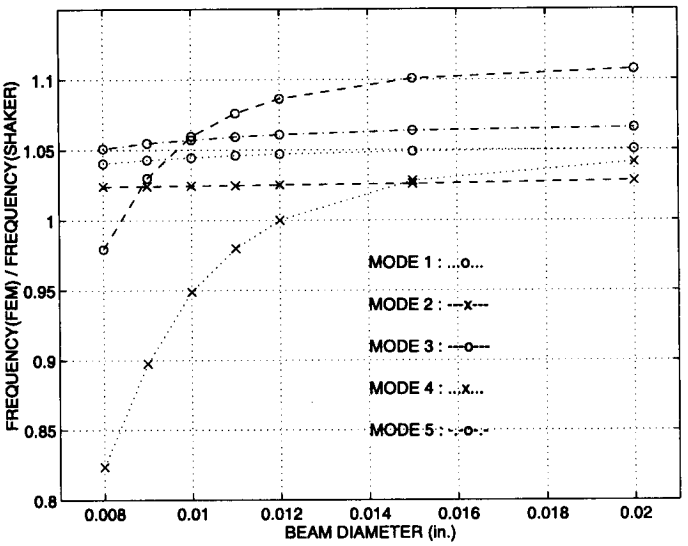

Fig. 14. Normalized frequencies versus d_e for the *B4D5R* panel (n = 4).

Table 5. Model parameters for the various panels with joints.

Panel type	n	de [x10^3 *in*]
L6D4H	4	45.0
L6D10H	1	70.0
L6D4R	8	67.0
L6D10R	8	40.0
B4D2H	1	17.0
B4D5H	1	13.0
B4D2R	8	12.0
B4D5R	8	8.50

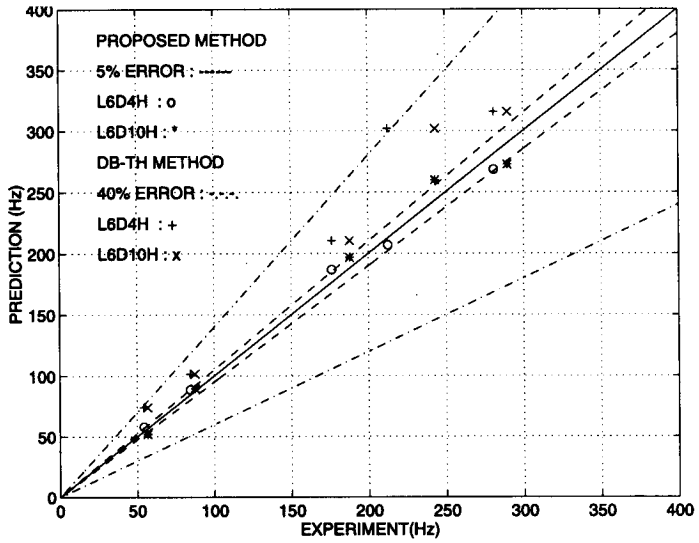

Fig. 15. Correlation between measured and predicted frequencies for *L6D4H* and *L6D10H* panels using the DB-TH and proposed finite element models.

sponding correlation for *B4D2H* and *B4D5H* panels. The 25% error observed for the BM-RF method is reduced to a 10% error for the proposed model.

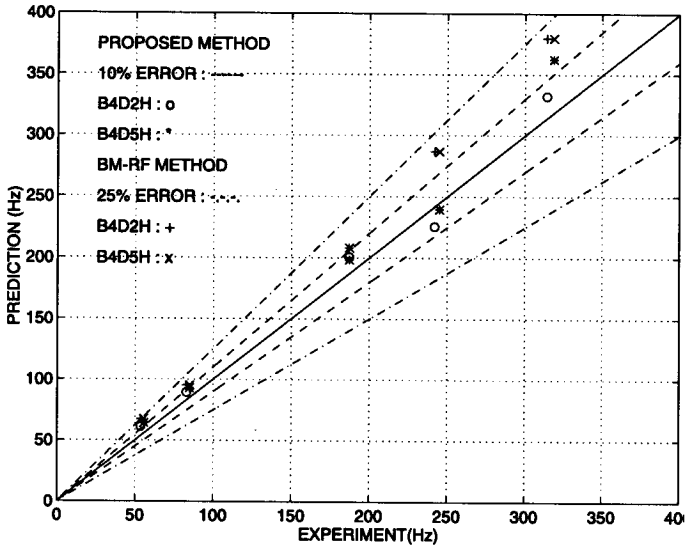

Fig. 16. Correlation between measured and predicted frequencies for *B4D2H* and *B4D5H* panels using the BM-RF and proposed finite element models.

The results for riveted panels *L6D4R* and *L6D10R* are shown in Fig. 17. Errors are reduced from 35% for the DB-TH method to 5% for the proposed model. Finally, Fig. 18 shows the results for *B4D2R* and *B4D5R* panels. The 15% error for the BM-RF method is reduced to 5% for the proposed model.

Conclusions

This paper has focused on the development of simple, improved numerical models based on a lumped parameter approach which accounts for joint flexibilities by a set of concentrated linear and torsional springs whose stiffnesses are experimentally determined. Simple tests were conducted on beam-like samples to determine the effective stiffnesses of these springs based on measured sensitivities for frequencies, mode shape tip

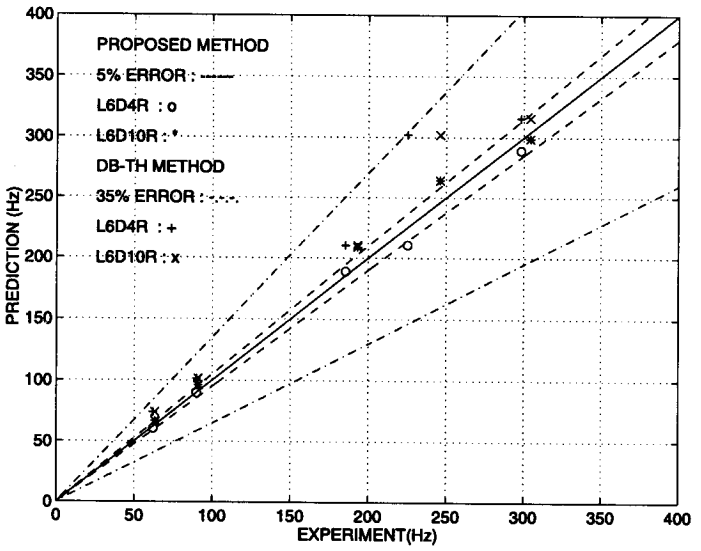

Fig. 17. Correlation between measured and predicted frequencies for *L6D4R* and *L6D10R* panels using the BM-RF and proposed finite element models.

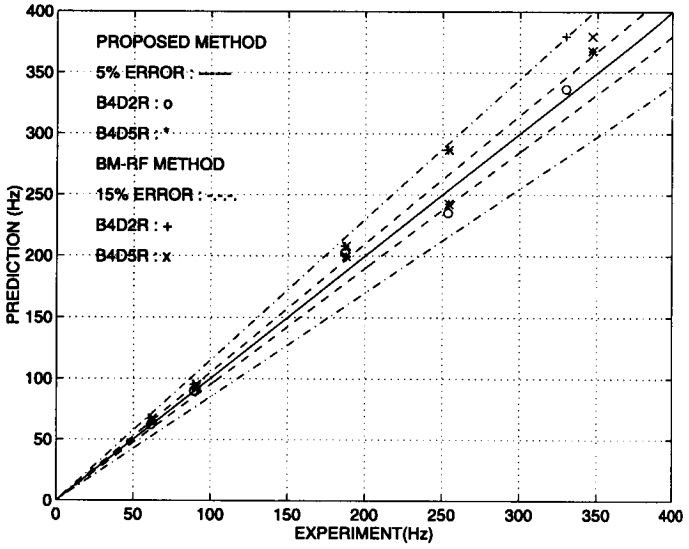

Fig. 18. Correlation between measured and predicted frequencies for *B4D2R* and *B4D5R* panels using the BM-RF and proposed finite element models.

deflections and mode shape tip slopes. The experimentally determined joint stiffnesses do not provide a unique value of stiffness in a specified direction, but rather, a range of reasonable values of joint stiffnesses.

The frequencies predicted by this proposed numerical model were compared with the measured frequencies for panels with various types of joints. The predictions based on this new model are considerably better than those based on current industry modeling practices: errors of up to about 40% obtained with the DB-TH or BM-RF method were reduced to about 5% with the proposed methodology.

Of course, the proposed finite element model, though based on a simple lumped parameter approach, involves a more complex representation of the joint area, and will require increased computational effort. However, the additional degrees of freedom associated with the improved representation of the joint could be condensed out to create a *joint element* that could be reused for all joints of the same type. This technique would involve minimum additional modeling requirements and costs.

Acknowledgments

This research was sponsored by the US Army Research Office, under Grant Number DAAH04-94-G-0073.

References

[1]Yun, S. H., and Bauchau, O. A., "Improving Modal Parameter Predictions for Jointed Airframe Panels. Part I: Experiments." *Journal of American Helicopter Society,* Vol. 43 (1), pp. 156-163.

[2]Nagy E. J., "Improved Method in Ground Vibration Testing." Proceedings of the American Helicopter Society Specialists' Meeting on Helicopter Vibration, Hartford, CT, pp. 452-464, 1981.

[3]Hughes, T. J. R., *The Finite Element Method: Linear Static and Dynamic Finite Element Analysis,* NJ, Prentice-Hall, pp. 310-379, 1987.

[4]Maruyama K., Yoshimoto I. and Nakano Y., "On Spring Constant of Connected Parts in Bolted Joint," *Bulletin of the JSME* , 18, pp 152-159, 1975.

[5]Motosh N., "Stress Distribution in Joints of Bolted or Riveted Connections." *Transactions of ASME,* pp.157-161, 1975.

[6]Cameron, P., Chasten, C. P. and Lu, L. W., "Prying and Shear in End-Plate Connection Design." *Journal of Structural Engineering, ASCE,* 118, p 1295-1311, 1992.